Applied Energy 111 (2013) 853–861

Contents lists available at SciVerse ScienceDirect

Applied Energy

journal homepage: www.elsevier.com/locate/apenergy

# Higher-capacity lithium ion battery chemistries for improved residential energy storage with micro-cogeneration ☆

K. Darcovich [a,*], E.R. Henquin [a], B. Kenney [a], I.J. Davidson [a], N. Saldanha [b], I. Beausoleil-Morrison [b]

[a] National Research Council of Canada, Energy, Mining and Environment Portfolio, Ottawa, Ontario, Canada K1A 0R6
[b] Dept. of Mechanical and Aerospace Engineering, Carleton University, Ottawa, Ontario, Canada K1S 5B6

## HIGHLIGHTS

- Characterized two novel high capacity electrode materials for Li-ion batteries.
- A numerical discharge model was run to characterize Li-ion cell behavior.
- Engineering model of Li-ion battery pack developed from cell fundamentals.
- ESP-r model integrated micro-cogeneration and high capacity Li-ion storage.
- Higher capacity batteries shown to improve micro-cogeneration systems.

## ARTICLE INFO

*Article history:*
Received 30 November 2012
Received in revised form 20 February 2013
Accepted 23 March 2013
Available online 21 June 2013

*Keywords:*
Building simulation
Lithium ion battery
High capacity cathode
Battery pack
Residential micro-cogeneration

## ABSTRACT

Combined heat and power on a residential scale, also known as micro-cogeneration, is currently gaining traction as an energy savings practice. The configuration of micro-cogeneration systems is highly variable, as local climate, energy supply, energy market and the feasibility of including renewable type components such as wind turbines or photovoltaic panels are all factors. Large-scale lithium ion batteries for electrical storage in this context can provide cost savings, operational flexibility, and reduced stress on the distribution grid as well as a degree of contingency for installations relying upon unsteady renewables. Concurrently, significant advances in component materials used to make lithium ion cells offer performance improvements in terms of power output, energy capacity, robustness and longevity, thereby enhancing their prospective utility in residential micro-cogeneration installations. The present study evaluates annual residential energy use for a typical Canadian home connected to the electrical grid, equipped with a micro-cogeneration system consisting of a Stirling engine for supplying heat and power, coupled with a nominal 2 kW/6 kW h lithium ion battery. Two novel battery cathode chemistries, one a new Li–NCA material, the other a high voltage Ni-doped lithium manganate, are compared in the residential micro-cogeneration context with a system equipped with the presently conventional $LiMn_2O_4$ spinel-type battery.



## 1. Introduction

Micro-cogeneration systems are making inroads for electricity generation at the residential level. The devices which provide both heat and power, known as the prime mover of the system, include internal combustion engines, solid oxide fuel cells, proton exchange membrane fuel cells, or Stirling engines (SEs). They typically generate less than 15 kW of electricity and are located within the household. When producing electricity alone, micro-cogeneration devices yield poor efficiencies, however when configured in systems which recover thermal energy generated in the electrical conversion process, the efficiency can rise to over 80%, referenced to the higher heating value of the fuel [1].

Annex 42 of the International Energy Agency's Programme on Energy Conservation in Building and Community Systems (IEA/ECBCSs) was focussed on reducing residential electric demand using micro-cogeneration devices through study with whole-building computer simulation software [2]. Among its conclusions were that engine start-up times, high operating temperatures, large thermal inertia, and internal controls preventing high thermal stresses, all contributed to sub-optimal response of micro-cogeneration systems to transient electrical loading. Accommodating these conditions would assist the transient performance of residential micro-cogeneration systems at times when electricity demand fluctuates rapidly. Forecasting into the future with high penetration rates of micro-cogeneration devices in households, it

☆ NRCC No. 53186. Crown Copyright © 2013.

* Corresponding author. Tel.: +1 613 993 6848; fax: +1 613 991 2384.
*E-mail address:* ken.darcovich@nrc-cnrc.gc.ca (K. Darcovich).

0306-2619/$ - see front matter © 2013 Crown Copyright and Elsevier Inc. All rights reserved.
http://dx.doi.org/10.1016/j.apenergy.2013.03.088

was concluded that the grid could no longer be viewed as an infinite power storage source. Thus, power storage technologies will become essential for residential micro-cogeneration applications.

The succeeding current IEA Annex 54 (www.iea-annex54.org) is expanding the scope of micro-cogeneration systems to also consider components contributing renewable electricity for the building. The temporal character of power generation from transient sources does not coincide with that for power consumption, thus electrical storage capacity is highly necessary for obtaining maximal energy use benefits and the best economy from these micro-cogeneration systems. Storing electricity in a rechargeable battery facilitates a quick transient response to a varying imposed electric load. Thus micro-cogeneration systems with residential energy storage (RES) are well positioned as a good solution for small-scale power generation, and the prospects are promising for scenarios with a large degree of market penetration.

Rechargeable large-scale lithium ion batteries with good capacity and cyclability are among the most promising choices for RES applications. Lithium ion batteries have many characteristics which make them highly suitable for being the electrical storage components of choice. These characteristics include very high energy density, good power output, good cycle life with a broad cycling range, high coulombic efficiencies and comparatively low heat output [3]. For prolonged intensive use, such as a in a micro-cogeneration system, proper control and management of a lithium-ion battery is crucial to ensure high capacity retention, as well as to operate the unit in a safe manner.

Current understanding suggests that lithium ion batteries at ratings around a 2 kW/6 kW h level are of a size suitable for development for residential power supply and storage. It has been shown that they can provide economic benefit under time-of-use pricing structures, as storing energy can reduce peak power demands as well as offset costly infrastructure upgrades to electrical power grid networks [4]. By simulating lithium ion battery physics and chemistry, the aim is to help identify microstructural properties and materials which will respond well to real imposed current loads which have been obtained from recent electrical profile measurements [5]. This approach can also help demonstrate a battery materials parameter set as a target for accompanying material development research to satisfy realistic operating requirements.

At present some large-scale commercial battery energy storage systems (BESSs) have been built and installed [6,7]. For now, at the beginning stages of the adoption of these technologies, economies of scale have not been achieved. Under present conditions, larger BESS systems are more economically viable, as the associated control equipment represents a significant fraction of the unit cost, and it does not increase in proportion with battery size. The battery management electronics for smaller storage systems contributes to their current high cost.

An avenue being pursued to rectify the high cost of BESSs is that of higher capacity battery materials. The quest for higher energy/power density lithium batteries has led to research on higher voltage cathode materials to replace the commonly used $LiMO_2$ (M = Co and Ni) and $LiMn_2O_4$ or even $LiMPO_4$ olivines (M = Fe and Mn). Substituted spinels of the family $LiMn_{2-x}M_xO_4$ (M = Cr, Ni, Cu, Co, and Fe) exhibit a significant capacity above 4.5 V.

Laboratories here at the National Research Council of Canada have had success in developing several of these kinds of materials, two of which are explored in this paper as examples of how improved battery materials can enhance RES units integrated into micro-cogeneration systems. First among these materials is $LiMn_{1.5}Ni_{0.5}O_4$ or LiNMO, which has a relatively high theoretical capacity of 146.7 mA h/g, almost all of which is around 4.7 V, and good cycling capability [8].

The second material, lithium nickel cobalt aluminum oxide ($LiNi_{0.8}Co_{0.15}Al_{0.05}O_2$ or LiNCA) is a leading candidate for lithium-ion batteries due to its high capacity and durability. The nominal voltage is 3.7 V, and the material capacity is in the 150–180 mA h/g range [9]. NCA is less commonly used in the consumer market. Its great potential as a cathode material has caught the attention of the automotive industry, despite safety and cost being current research issues.

Table 1 presents some cost figures related to materials costs for the three cathode materials considered here [10]. The LiNCA material is significantly more costly on a weight basis compared to the other two materials, owing to the high cost of its cobalt component. The cost per unit of current output however is still higher, but still more or less in line with the other two materials, since the cathode represents only one part of the total cell cost.

Residential energy use studies typically employ whole building simulation tools such as ESP-r to explore operational scenarios and system configurations in order to provide informed comment and recommendations for the suitability of their implementation [11]. ESP-r whole building simulations are used to coordinate all energy related components to evaluate usage scenarios for determining best practices in terms of energy consumption and economics. Strengths of ESP-r include its ability to handle complicated heat flux and plant equipment, as well as its ready availability and open-source format suitable for adding simulation capabilities and models for new technologies [12]. A number of cases can be cited from the literature where building simulations for improving energy efficiency have been studied with systems which included batteries for electrical storage. The concept of including storage batteries with supplementary residential power generation sources has been understood for some time now, an early example provides qualitative discussion about the general applicability of batteries with PV power [13].

Micro-cogeneration models using battery storage for load levelling applications have been developed using lead acid batteries [14]. However, in favor of Li-ion technology, life-cycle analysis has demonstrated the poor economic viability of competing lead acid battery technology [15]. An electric storage model in the building simulation program ESP-r using lead acid and vanadium redox flow batteries (VRFBs) has also been developed [16], which studied battery use coupled with photovoltaic renewable generation, within the power-modeling domain of ESP-r. The present subject is of broader interest, as it has been extended to energy studies of battery use on the community scale, but to this point, has not been coupled with the electrochemical fundamentals more representative of real battery behavior [17].

The main theme of this present work is to present some analysis of the performance of a micro-cogeneration system consisting of a Stirling engine as the combined heat and power (CHP) prime mover, along with a large Li-ion battery for energy storage and provision, according to the varying temporal demands of an annual electrical load profile. The inclusion of the battery in the system allows for less overall draw from the grid, as well as the storage of any temporary excess of electricity for use at a later time. A further theme is to show that by demonstrating improved battery performance through simulating discharge properties of novel higher-capacity cathode materials, the prospects for the viability of such CHP systems with batteries are much enhanced.

**Table 1**
Comparison of material costs for the three cathode formulations [10].

| Material | Capacity (mA h/g) | $/kg | $/A |
|---|---|---|---|
| $LiMn_2O_4$ | 110 | 16 | 0.145 |
| LiNCA | 180 | 40 | 0.222 |
| LiNMO | 147 | 25 | 0.170 |

A novel contribution of the present work is to incorporate and scale-up the measured fundamental electrochemical behavior of a Li-ion cell, to produce a new Li-ion battery pack component module for use with the ESP-r software. This new ESP-r module then made it possible to simulate the performance of a Li-ion battery in a micro-cogeneration system with a SE as prime mover. Cases were explored and evaluated for two new high-capacity battery chemistries, and compared with the performance of the same system using the conventional $LiMn_2O_4$ battery chemistry.

The objectives of this present paper can be stated as follows. First, charge–discharge curves for LiMNO and LiNCA batteries for a range of currents up to 1C (i.e., a current that would discharge the battery in one hour) were to be determined experimentally. Parameter estimates could be then made for some of the electroceramic properties of LiNMO and LiNCA to allow transport based electrochemical discharge simulations of these batteries to be run at a broader range of currents required to be representative of real residential electrical power loads. These electrochemical simulations provide an extended set of charge–discharge curves, which will serve as the basis for creating an ESP-r battery module representing each of these two novel types of Li-ion battery materials. The above work serves to prepare the required inputs for the comparison of the annual energy performance of a micro-cogeneration system consisting of a SE with a Li-ion battery for electrical storage, with respect to measured electrical demand profiles, for three cases. The first, is the reference case which has a Li-ion battery with a $LiMn_2O_4$ cathode material, and it is then compared to two prospective cases where the Li-ion battery is made with either LiNMO or LiNCA high capacity cathode materials.

While renewable energy sources were mentioned in the introduction of the present study, they are not included in this work, which compares novel battery materials in a simulation scenario which had previously been conducted without renewables [18]. It is understood that the addition of a renewable component to a micro-cogeneration system presents an even stronger case for the benefits of using Li-ion batteries for RES.

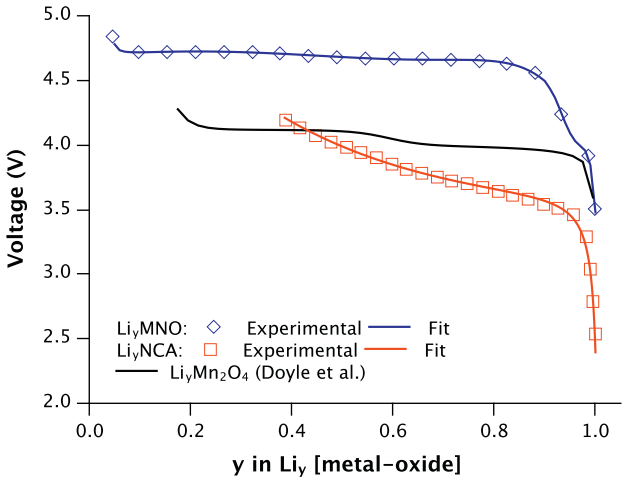


**Fig. 1.** Comparison and polynomial curve fits of OCV curves collected galvanostatically at a rate of C/50 for LiMNO and LiNCA active materials alongside that of $LiMn_2O_4$.

## 2. Experimental

Electrochemical cells (2325 size coin cells) were used to collect open-circuit voltage (OCV) data for porous LiNCA and LiMNO cathodes with lithium-foil counter electrodes. Commercial LiNCA (Toda Materials, Japan) and in-house synthesized LiMNO powders were used. The synthesis and phase purity of the LiMNO has been reported by Duncan et al [8]. The porous cathodes were made from a slurry containing 92% active material, 3% Super-S carbon, 3% poly (vinylidene fluoride (PVDF) binder dissolved in *n*-methyl pyrrolidone, all by weight. The slurry was cast onto an aluminum foil using an automated doctor blade spreader and dried in a convection oven at 80 °C for 3 h and then in a vacuum oven at 80 °C for 12 h. Electrode disks of 12.7 mm diameter were punched from the coated foil and pressed at 1.0 ton pressure using a uni-axial press. The cells were assembled with Li foil punched in 15.9 mm disks as the counter electrode and 1 M $LiPF_6$ in a 3:7 mixture of ethylene carbonate (EC) and diethyl carbonate (DEC) as an electrolyte with two layers of microporous propylene separators (Celgard 2500). To collect the open circuit voltages as a function of the state-of-charge (or lithiation of the active material), these cells were galvanostatically cycled at rates of C/12 for 5 cycles and then at a rate of C/50 using Arbin battery cyclers, where C was defined as the practical capacity, based on previous measurements with the same material, 180 mA h/g for LiNCA and 120 mA h/g for LiMNO. For the high-voltage LiMNO samples, the cells were cycled between a voltage of 4.9 V and 3.5 V and for the LiNCA samples, the voltage was 4.2–2.5 V. The C/50 experimental data were fit with a rational polynomial. These functions were required in the electrochemical cell model to provide reference potentials in discharge simulations. Fig. 1 shows the measured OCV curves.

## 3. Modeling overview

Two different modeling procedures are employed in this project. They are detailed below. The first was a fundamentals based electrochemical transport model of discharge in a single Li-ion cell which is presented in more detail in Section 3.1. Output from a range of currents from this basic model was collected and condensed into an engineering type empirical model to represent the function of a Li-ion battery pack operating as a RES unit in a residential micro-cogeneration system. The engineering-level model is based on an equivalent circuit representation of a battery, and is presented in Section 3.2. This equivalent circuit model can be used for simulating battery packs of consisting of multiple cells, and can be interfaced with residential energy use simulations.

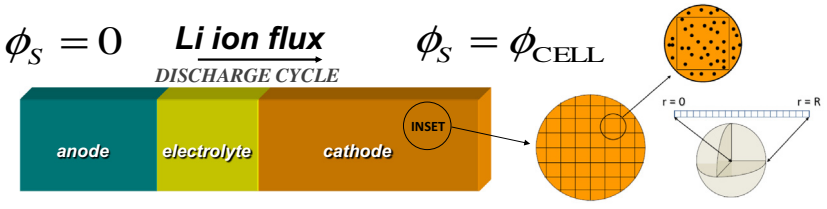


**Fig. 2.** One-dimensional configuration of the lithium ion battery for the discharge simulation. Inset shows spherical pseudo-domain representing average solid electrode particle interior located at grid position in cell layer.

### 3.1. Cell discharge sub-model

A lithium ion battery consists of three specially constituted layers, namely, an anode where lithium ions are stored for discharge, a separator, to preserve the charged state when the battery is not in use, and the cathode, to collect and store the lithium ions arriving during discharge. As such, a lithium ion battery converts chemical potential to electrical current. The active materials inside the electrode layers are small solid particles which are suspended in a conductive polymer electrolyte phase which also composes the separator layer. A diagram of a simplified lithium ion battery configuration is shown in Fig. 2. The suspended solid electrode phase which has its own local spherical coordinate system is depicted in the inset of Fig. 2.

The case developed here has its foundation in theory developed by Newman and Tiedemann [19], and subsequent numerical models [20,21]. Full details of the physical basis for the model may be found in [4,20,21]. An abbreviated description of the underlying physics of the model follows.

The cell potential exists because of the differing states of chemical potential resident in the two electrodes. When the circuit is closed, the current ($I_{app}$) arising from an imposed power draw will produce a corresponding lithium ion flux. The following discussion details the set of coupled partial differential transport equations which govern the discharge (and charge) behavior of a Li-ion battery. Below, the subscript $S$ refers to the solid material in the electrode phase, while the subscript $E$ refers to the material in the electrolyte phase. In the equations below, $R$ is the gas constant, $T$ is the temperature, $t$ is time, and $F$ is Faraday's constant.

The electrical potential in the solid phase, $\phi_S$, is given by

$$\nabla \cdot (-\kappa_S \nabla \phi_S) = -S_a j_{loc} \tag{1}$$

where $\kappa_S$ is the effective conductivity [21], $S_a$ is the specific surface area of the electrode interface and $j_{loc}$ is the interphase transfer current density.

Eq. (1) has the boundary conditions:

$$\nabla \phi_S = \frac{-I_{app}}{F\sigma_S} \text{ on the terminals,}$$

$$\nabla \phi_S = 0 \text{ on separator boundaries}$$

An additional condition was to set $\phi_S = 0$ at the anode terminal as a reference value, thus enabling the determination of the cell potential as the difference between the $\phi_S$ values at the two battery terminals.

The electrical potential in the electrolyte phase, $\phi_E$, is given by,

$$\nabla \cdot \left( \kappa_E \left[ -\nabla \phi_E + \frac{2RT}{F}(1-t_+)\frac{1}{c_E}\nabla c_E \right] \right) = S_a j_{loc} \tag{2}$$

where $\kappa_E$ is the effective conductivity [21], $t_+$ is transference number and $c_E$ is the lithium ion concentration. For Eq. (2), $\nabla \phi_E = 0$ on all boundaries.

The lithium ion concentration in the electrolyte phase, $c_E$, is given by,

$$\epsilon \frac{\partial c_E}{\partial t} + \nabla \cdot \left( -D_E^{eff} \nabla c_E \right) = -\frac{S_a j_{loc}(1-t_+)}{F} \tag{3}$$

where $\epsilon$ is the volume fraction of electrolyte phase, and $D_E$ is the effective diffusion coefficient [21]. For Eq. (3), $\nabla c_E = 0$ on all boundaries.

The lithium ion concentration in the solid phases, $c_S$, solved on a separate pseudo-domain over the internal radius $r$, of the solid particle, assumed to be spherical.

$$\frac{\partial c_S}{\partial t} + \frac{1}{r^2}\frac{\partial}{\partial r}\left( -r^2 D_S \frac{\partial c_S}{\partial r} \right) = 0 \tag{4}$$

For Eq. (3), the boundary conditions are,

$$\frac{\partial c_S}{\partial r} = 0 \quad \text{at } r = 0 \quad \text{and} \quad \frac{\partial c_S}{\partial r} = \frac{-j_{loc}}{D_S} \quad \text{at } r = R$$

The interphase ion lithium ion flux, $j_{loc}$, is given by

$$j_{loc} = i_0 \left( \exp\left(\frac{\eta F}{RT}\right) - \exp\left(\frac{-\eta F}{RT}\right) \right) \tag{5}$$

In Eq. (5), $\eta = \phi_S - \phi_E - \phi_{ref}(c_{S,\ surf})$, and the term $i_0 = k_0\sqrt{c_E(c_{S,max} - c_{S,surf})c_{S,surf}}$. The value $\phi_{ref}(c_{S,\ surf})$ is an equilibrium reference potential, determined at the solid phase material at the state of charge corresponding to the surface lithium ion concentration. Values for $c_{S,max}$, the maximum solid phase ion concentrations are from Table 2 of Ref. [21].

The applied current density, $I_{app}$ is set at a constant value, representing the imposed load on the battery. It is partitioned through the two phases, so that,

$$I_{app} = i_E + i_S \tag{6}$$

Explicitly, by Ohm's Law, it can be stated,

$i_S = -\sigma_S \nabla \phi_S$ and, the relation between current and potential in the electrolyte phase is,

$$i_E = -\kappa_E^{eff}\nabla \phi_E + \frac{\kappa_E^{eff} RT}{F}(1-t_+)\frac{1}{c_E}\nabla c_E$$

The current transfer at the terminals occurs entirely via the solid phase, such that at $i_S = I_{app}$. Conversely, the electrode phase disappears at the separator interface, so at the electrode–separator boundaries, $i_E = I_{app}$.

On the basis of the configuration shown in Fig. 2, a 100 cell one-dimensional grid was made for the numerical transport model as described above. A CFD-type transport based model which solved the simultaneous set of transport equations outlined in Eqs. (1)–(6), was developed and implemented with the finite-volume method to solve the equation set required to simulate discharge and charging processes in a Li-ion cell [4]. A sphere representative of the solid electrode phase was included in the model as a local pseudo-phase in each grid cell, in order to provide a radial Li-ion concentration profile. The average Li-ion concentration inside an electrode particle can differ widely from the Li-ion concentration at the particle interface with the electrolyte phase, and it is this interfacial concentration value which is important for accurate electrochemical modeling [19].

#### 3.1.1. Battery material parameters

For its active materials, the battery is modeled with properties from $LiC_6$ solid particles in the anode region, and one of either $LiMn_2O_4$, LiNCA or LiNMO solid particles in the cathode region. The electrolyte phase is taken as 2:1 volume basis mixture of ethylene carbonate and dimethyl carbonate [21]. Material morphological parameters, expressions for conductivity, diffusion constants, material properties, open circuit potentials and reaction kinetic constants are given in [4,20,21]. The battery model took dimensions from a small coin cell type device with an anode thickness of 100 μm, a separator thickness of 52 μm, and a cathode thickness of 174 μm. A constant temperature of 25 °C was assumed. For the model validation against data from [21] the applied current den-

**Table 2**
Depth of discharge potential range for the cathode materials.

| Cathode | $\phi_{DOD=0}$ (V) | $\phi_{DOD=1}$ (V) |
|---|---|---|
| $LiMn_2O_4$ | 4.22 | 3.15 |
| LiNCA | 4.15 | 2.77 |
| LiNMO | 4.72 | 3.43 |

sity was 1.75 A $m^{-2}$, while for the full scope of the project, current densities ranging from 0.01 to 140 A $m^{-2}$ were simulated.

### 3.1.2. Numerical implementation

The model described above was implemented numerically with the open-source software OpenFOAM (Field Operation And Manipulation), which is an object-oriented high level code designed for treating problems which can be represented by partial differential field equations [22]. The discharge process is modeled across a single battery layer (i.e., Fig. 2), using a one-dimensional 100 element grid. Time steps of 0.1 s were chosen. For each time step, the first part the solution was to solve the current–potential field comprising the set of instantaneous variables,$\phi_S$, $\phi_E$ and $j_{loc}$ with an iterative algorithm. This part of the solution was based on the battery state of charge, and determined a rate value ($j_{loc}$, mol $m^{-2}$ $s^{-1}$) which was then used to solve the temporal equations for $c_E$ and $c_S$. The basic physical behavior and simulation outputs from the battery discharge submodel are detailed in [4].

An established cathode material is the spinel-type $LiMn_2O_4$, with capacity around 110 mA h/g, well characterized in the literature [20,21]. Discharge curves for $LiMn_2O_4$ are shown in Fig. 3a, followed by data and simulated results for LiNCA (Fig. 3b) and LiMNO (Fig. 3c). In all cases, the anode is $LiC_6$ graphite, with $LiPF_6$ salt in the electrolyte. The cells constructed with two new cathode materials have improved electrolyte properties compared to the ethylene carbonate/dimethyl carbonate mixture used in the spinel case.

## 3.2. Lithium ion battery ESP-r module

A battery pack consists of the same kind of basic layers described in Section 3. The battery capacity is directly proportional to the total area of the layers put into the pack. Battery packs configure individual cells in combinations of serial and parallel arrangements in order to achieve current and voltage requirements.

An engineering-type empirical lithium-ion battery pack model based on cell discharge behavior is developed for the present project as described below. According to Gao et al., battery charge and discharge processes can be empirically represented with a lumped capacitance assumption and state variables [23] As a starting point, a reference curve is determined by from a polynomial fit of the open-circuit voltage (OCV) as function of the battery depth of discharge (DOD). The depth of discharge is a parameter assigned to the battery to indicate the degree to which it has been discharged. It is a somewhat arbitrary parameter, the range of 0–100% discharge corresponds to the imposed upper and lower operating voltage limits on the battery. These limits are selected with a view of maintaining lithium levels in the electrodes in states where the active material remains stable and can cycle indefinitely without excessive material degradation occurring. The DOD range was defined by the potentials given in Table 2.

At different currents, there is a shift of the voltage as a function of DOD, represented by the internal resistance multiplied by the current [18]. The ratio of battery capacity corresponding to the OCV curve and battery capacity corresponding to discharge curve at a given higher current is the parameter $\alpha$ in the Gao model.

This property is exploited through Eq. (7), as a means of updating the DOD given a specified battery state and load.

$$\frac{d\mathrm{DOD}}{dt} = \frac{-I(t)}{\alpha\beta \mathrm{CAP}_{\mathrm{REF}}} \tag{7}$$

In Eq. (7), $\beta$ is a factor for battery temperature, and $\mathrm{CAP}_{\mathrm{REF}}$ is a battery reference capacity based on the cathode capacity, and scaled to

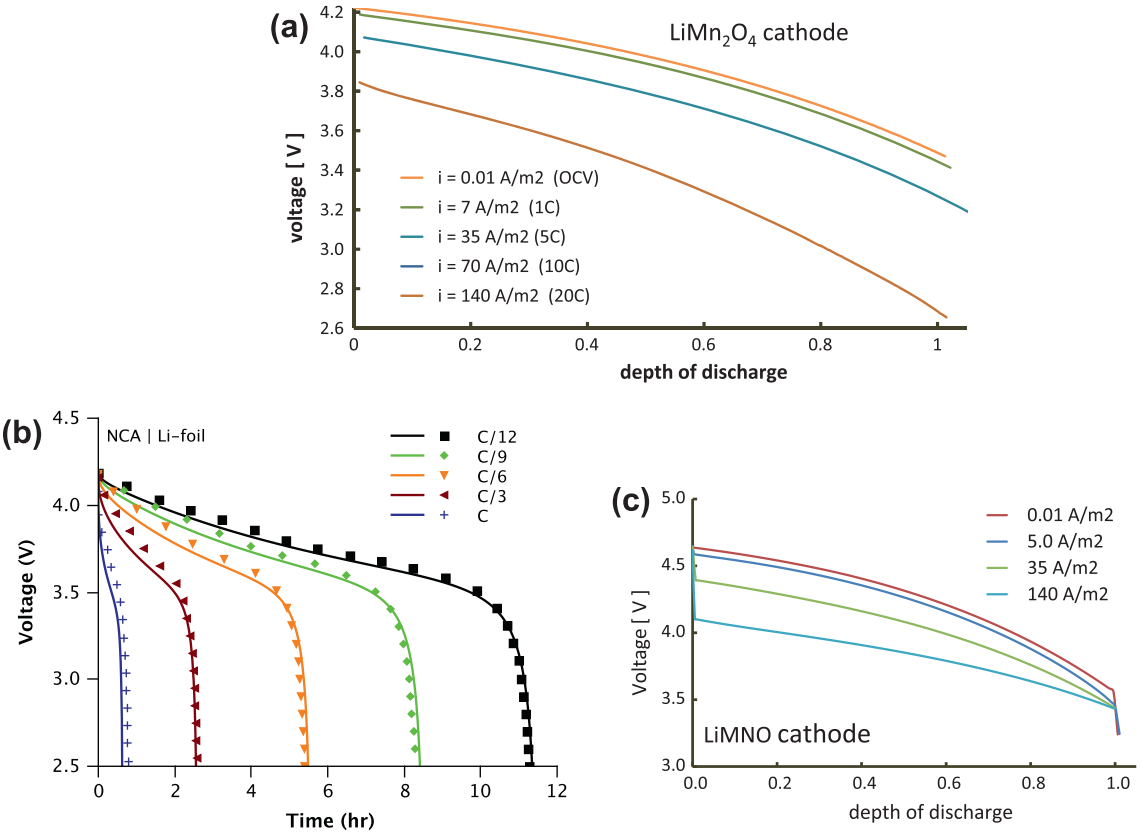


**Fig. 3.** Simulated battery discharge curves based on measured OCV curves. (a) $LiMn_2O_4$ spinel. (b) LiNCA, 1C ≈13.4 A/$m^2$. This data is also fitted against experimental measurements. (c) LiMNO.

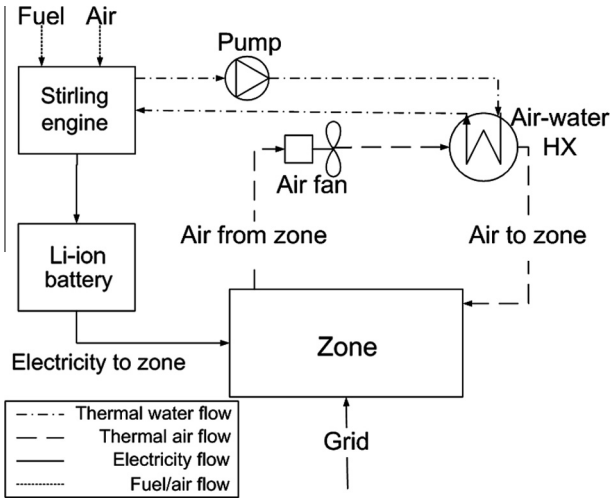


**Fig. 4.** Plant system schematic for application demonstration.

reflect the net size of the battery pack. These parameters are explained in more detail in [18]. The battery potential is then expressed relative to the reference curve through use of multiplicative factors which depend on the imposed current and battery state of charge. These factors must be uniquely determined for each battery chemistry. A temperature dependant functionality can also be imparted to the model.

The voltage during discharging can be expressed as:

$$V(t, DOD, I(t)) = OCV(DOD) - I(t)R_{\text{int}}(DOD) \quad (8)$$

where $I(t)$ is the current (amperes) and $R_{\text{int}}$ is the internal resistance (ohms).

Simulations in ESP-r occur at discrete time-steps in a quasi-steady-state fashion within the time interval. The battery parameters are considered constant over the course of a time-step. Under transient load, the current is updated for the next time-step. An imposed power load $P$ (where $P = IV$), determines a required current $I(t)$ based on the cell voltage.

Applying this current over a time step will advance the DOD (Eq. (7)), and correspondingly cause a small voltage drop (Eq. (8)).

It should be noted that simulated data (i.e., Fig. 4a–c) are required as input to implement the Gao model, as it depends on knowing the battery state of charge, a variable that is it not readily available from experimental measurements, but which were determined from the solid phase lithium ion concentration fields in the transport based battery sub-model.

The required battery pack was constructed of small basic cells with a capacity of 1.80 A h. These would be in line with $LiMn_2O_4$ 18,650 cells [24]. In terms of battery architecture, the for a pack of 6 kW h at 120 V called for a configuration of 35 in-series sets of 34 cells in parallel, a total of 1190 individual cells.

### 3.3. Integrated system

To demonstrate the performance of Li-ion batteries for residential storage considered in this work, a model of a house was created in ESP-r for an annual simulation. The layout of the house was basic: a single-zone, rectangular house located in Ottawa, Canada. The model used typical constructions to represent the houses walls, ceiling and floor. It had a floor space of 132 $m^2$ and a volume of 528 $m^3$. These values were chosen to represent a typical Canadian single family detached dwelling [25].

A SE (Whisper Tech Ltd. WhisperGen Stirling engine, fueled by natural gas), represented in a model developed by Ferguson, was used as the micro-cogeneration device in the simulation [26]. Weather data taken for the year 2008 in Ottawa, Ontario, Canada [27] provided the external environment for the simulation. A schematic of the plant configuration used in the simulation is shown in Fig. 4. The SE was configured to constantly produce 900 W of electricity for the house throughout the year. The useful heat recovered by the engine was circulated via a pump to an air-to-water heat exchanger. The air-to-water heat exchanger, driven by a fan, supplied warm air to the household. The pump and the fan consumed 50 W and 25 W of electricity, respectively.

The household electrical demands were input as combined non-HVAC and space cooling loads on a 5-min basis. Data from a medium-level energy use house from a Carleton University field data collection project served as the power use profile [5]. The battery was inserted into the system to buffer energy demand and improve efficiency. Under the battery management logic devised for the simulations, if the combined electricity demand from the household, pump and fan was less than the production from the stirling engine, the battery would charge with the excess electricity produced. If the SE and battery could not meet the combined electric demand, electricity would be imported from the grid. Likewise, if electricity production from the stirling engine was greater than the combined electric demand and the battery was fully charged, the excess electricity was exported to the grid. Finally, if the thermal demands of the household exceeded the heat produced by the SE, an auxiliary natural gas burner, not shown in Fig. 4 provided the necessary heat.

## 4. Results and discussion

A number of scenarios have been explored using the integrated model outlined above [18]. A number of beneficial effects resulted

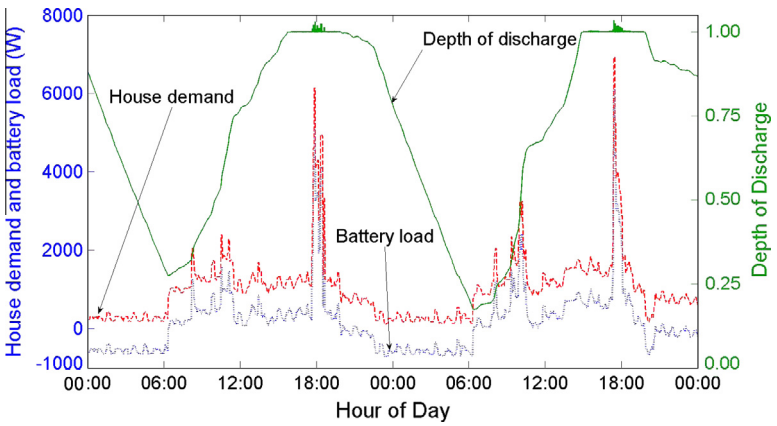


**Fig. 5.** Household electricity demand, $LiMn_2O_4$ battery load and battery DOD over two days of simulation beginning August 4th, 2008.

from the inclusion of a lithium ion battery in a micro-cogeneration configuration. The first example considers the integrated system with the conventional $LiMn_2O_4$ cathode material. In this case, the house electrical demand and battery load over two summer days as depicted in Fig. 5, shows that the production of the SE during overnight periods was able to satisfy the household power demand and charge the battery with its excess electricity production. Over the daytime, the household electricity demand increased above the production of the SE and the battery began to discharge to help manage the power load and reduce power draw from the grid. The inclusion of a RES in a micro-cogeneration system reduced the extent of grid interactions with the home.

A similar scenario as presented in Fig. 5 was next simulated with battery packs of the same size made with the novel LiNCA and the LiMNO cathode materials. It would be expected that the benefits of battery use with micro-cogeneration would improve in proportion to the pack capacity. Note that while Fig. 5 was shown as an example of the system behavior, different dates were chosen for Figs. 6 and 7 where the demand peaks were shorter and broader, and better illustrate the differences and benefits of the batteries with the higher-capacity cathode materials and some of the design corrections taken to improve the performance.

Fig. 6 compares the micro-cogeneration performance of same size batteries with the three different cathode materials. What can be seen here in this initial instance is that the increased capacities of the LiNCA and LiNMO batteries do not seem to show appreciable benefits in this scenario. Fig. 6 reveals that an integrated design of all the equipment in the configuration must be undertaken in order to attain a more optimal performance with the micro-cogeneration system. The shortcomings shown in Fig. 6 arise from a mismatch between the power output from the SE and the battery capacity. A 900 W SE cannot fully recharge the conventional battery nor the higher capacity batteries during the off-peak charging periods under the battery management system as provided. The battery load for the two higher capacity batteries is essentially identical to that of the conventional battery with an $LiMn_2O_4$ cathode. There is still a minor benefit from the higher capacity materials, in that they do not cycle as deeply, and will thus show a longer service life under the scenario of Fig. 6.

A possible adjustment to improve the system performance would be to decrease the size of the battery, such that the $LiMn_2O_4$ battery could be properly charged during the off-peak periods. In preliminary tests with smaller capacity cells where this does occur, it was still found that the reduced battery pack size leads to a

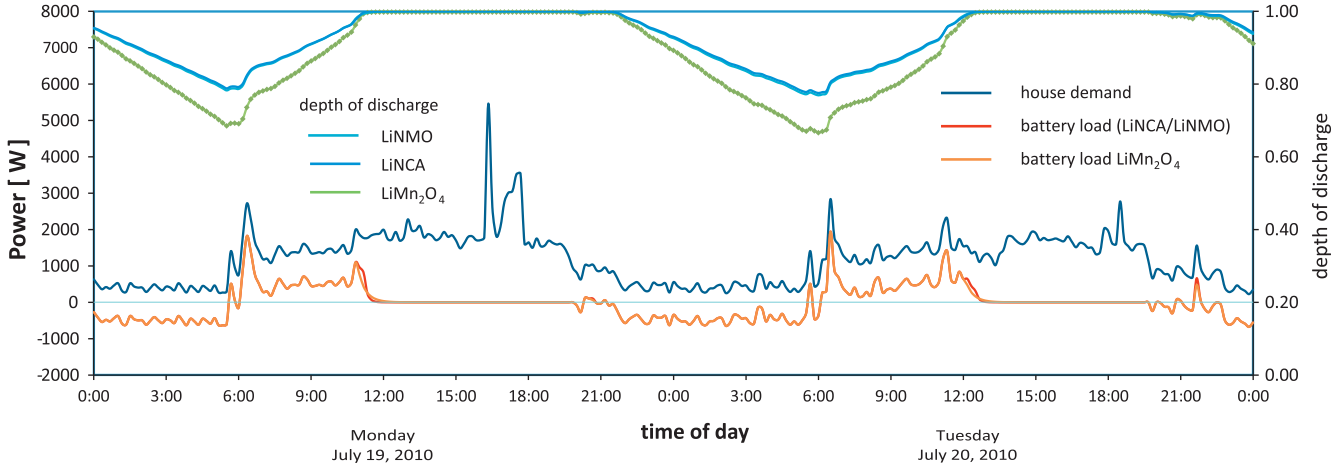


**Fig. 6.** Comparison of household electricity demand, $LiMn_2O_4$, LiNCA and LiMNO battery load and battery DOD over two days of simulation beginning August 4th, 2008.

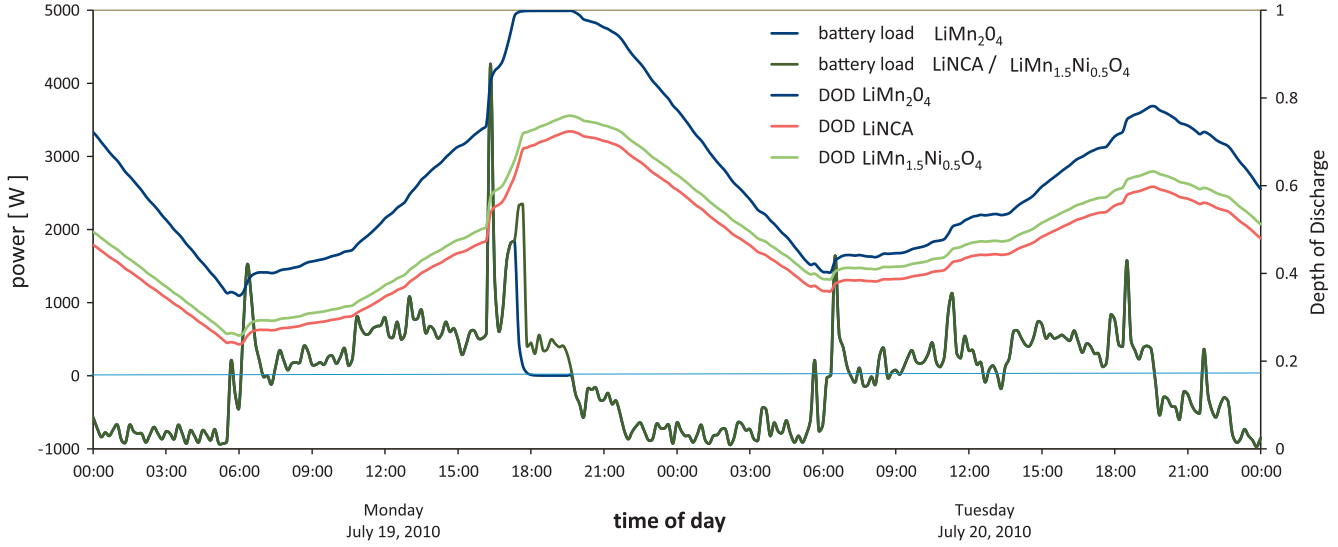


**Fig. 7.** Comparison of household electricity demand, $LiMn_2O_4$, LiNCA and LiMNO battery load and battery DOD over two days of simulation beginning July 19, 2008. In this case the SE capacity is 1200 W.

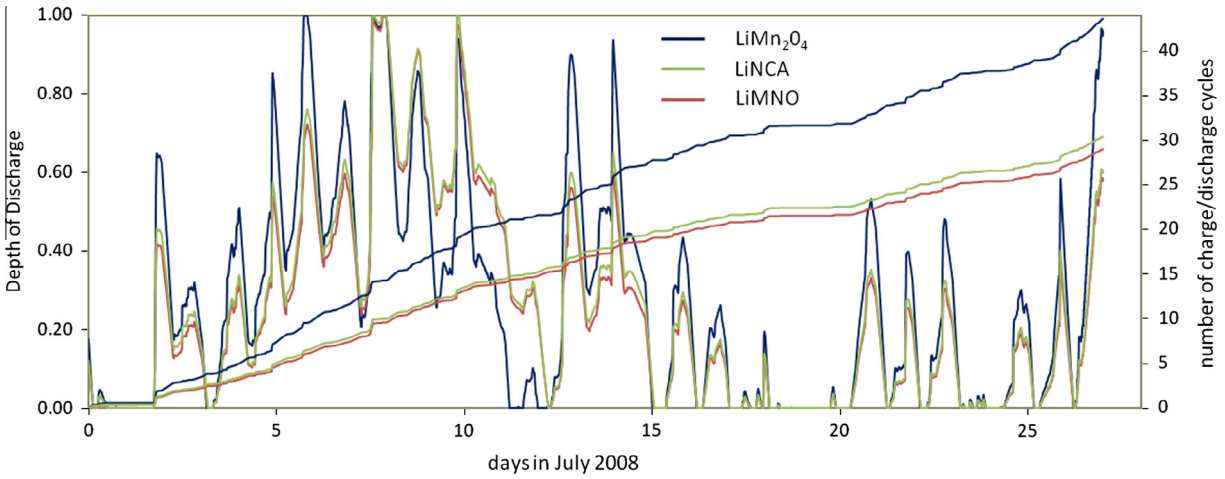


**Fig. 8.** Battery pack depth of discharge profiles and cumulative total of discharge cycles over the month of July 2008, based on micro-cogeneration system with 1200 W Stirling engine and 1190 cell battery pack.

very rapid battery discharge, including when simulated with the LiNCA and LiMNO batteries, despite their higher capacity.

A number of simple preliminary simulations confirmed that the electrical load required of the battery was simply too great to be provided by cells ranging from 1.2 kW h up to 6 kW h capacity in the existing micro-cogeneration configuration. In a sense, this was an obvious consequence, but the point of the exercise was to check if the higher capacity batteries could offer any advantage in this situation. They did not.

Another approach with the same logic of decreasing the battery capacity ratio to SE power output was taken for exploring a two day scenario. Here, the system was modified by enlarging the SE. From the year-long data set, the two consecutive days beginning July 19, 2008, were found where the discharge was near complete at the start of the cycle. Starting from a near fully discharged state puts the battery capabilities in higher relief for demonstrating their performances.

A power output of 1200 W was selected for the simulation. This larger SE is capable of providing sufficient charge to the higher capacity LiNCA and LiMNO batteries, such that some of the peak periods of the daily demands can be met without reaching a full depth of discharge. Fig. 7 shows this simulated scenario. The other benefit of this configuration is that the higher capacity batteries cycle through a smaller part of their capacity range, thereby putting less net stress on the battery materials which will serve to extend the useful lifetime of these batteries. Fig. 8 shows a month long simulation for the system shown in Fig. 7, where the depth of discharge is recorded as well as a total number of battery cycles. For the cases of incomplete cycles, one cycle was calculated on current-based stoichiometric equivalents of the full battery capacity.

It was not the intention of the present project to exhaustively explore a large number of micro-cogeneration scenarios in order to identify the conditions where the present combination of components can be operated optimally. The point to be made is that with the present trend of improvements in battery materials, the prospects for Li-ion technology to be used in a RES context are indeed promising. From the results of the simulations that are partially depicted in Fig. 8 the $LiMn_2O_4$ battery used approximately 800 cycles over the year. If the long-term industry goal of a 10,000 cycle life span can be realized this would equate to a service lifetime of more than 12 years [28]. For the LiMNO and LiNCA battery chemistries, the expected service life would be 17 and 18 years respectively.

In a best case scenario, where the all the heat energy provided by the Stirling engine could be used, micro-cogeneration with a lithium ion battery under the conditions outlined in [4] can reduce daily power consumption from the electrical grid by 30% from 61 kW h to 43 kW h, at a cost savings of about $CAD440/year. Annual cost savings with the same sized batteries under this use scenario with the LiNCA and LiMNO cathodes would be about $CAD750/year and $CAD690/year respectively.

## 5. Conclusions

A fundamental transport based model of the function of a lithium ion battery has been used to provide the necessary inputs to create a battery module based on the Gao equivalent circuit model in ESP-r for residential energy storage. The purpose of this battery simulation module was for the performance assessment of large scale storage batteries operating in a micro-cogeneration system, and to show that making batteries using from novel advanced high-capacity battery cathode materials significantly enhance the economic viability of such systems.

The present study evaluated annual residential energy use for a typical Canadian home connected to the electrical grid, equipped with a micro-cogeneration system consisting of a Stirling engine for supplying heat and power, coupled with a nominal 2 kW/6 kW h lithium ion battery. The energy performance of two novel battery cathode chemistries, one a new Li–NCA material, the other a high voltage Ni-doped lithium manganate, were compared in the residential micro-cogeneration context with a system equipped with the presently conventional $LiMn_2O_4$ spinel-type battery. It was found that the complex nature of a multi-piece micro-cogeneration system benefits to a great extent from usage scenario simulations due to the specific capacities and outputs of the components. Since the sizes and performance of the components are not continuously scalable, energy use simulation was shown to be an effective means to recommend the details of system configurations for specific cases. It was also found that the prospects for Li-ion technology for residential energy storage are positive, stemming from novel of battery materials advances. Higher capacity cathode materials such as LiMNO and LiNCA will extend battery pack service lives upwards of 30%, and will be a key factor in their eventual commercial viability.

Analysis of using large batteries in building environment simulations clearly demonstrate how expected demands on large-scale batteries for residential energy storage assist in sizing and configuring components for optimal use in micro-cogeneration systems. Continued materials research and engineering know-how derived

from this work will serve to enable the realization of cost-effective large-scale lithium ion batteries for residential energy storage.

## Acknowledgments

Funding from Natural Resources Canada, Program on Energy Research and Development (PERD) Project 5.1.2-F22, Energy Conversion and Storage, is gratefully acknowledged.

## References

[1] Knight I, Ugursal I. Residential cogeneration systems: a review of the current technologies. IEA/ECBCS annex 42; 2005.
[2] Beausoleil-Morrison I. An experimental and simulation-based investigation of the performance of small-scale fuel cell and combustion-based cogeneration devices serving residential buildings. IEA/ECBCS annex 42 report; 2008.
[3] Scrosati B, Garche J. Lithium batteries: status, prospects and future. J Power Sources 2010;195(9):2419–30.
[4] Darcovich K, Gupta N, Caroni T, Davidson IJ. Residential electrical power storage scenario simulations with a large-scale lithium ion battery. J Appl Electrochem 2010;40(4):749–55.
[5] Saldanha N, Beausoleil-Morrison I. Measured end-use electric load profiles for 12 Canadian houses at high temporal resolution. Energy Build 2012;49:519–30.
[6] Acquati A. APS to test energy efficient substation in Flagstaff. Northern Arizona News; March 20, 2012.
[7] DasGupta R. Substation installations of electrovaya's MW h-scale lithium-ion superpolymer®. Batteries for smart grid applications. In: PRiME 2012, 222nd meeting of the electrochemical society. Honolulu, Hawaii; October 7–12, 2012.
[8] Duncan H, Abu Lebdeh Y, Davidson IJ. Study of the cathodeelectrolyte interface of $LiMn_{1.5}Ni_{0.5}O_4$ synthesized by a sol–gel method for Li-ion batteries. J Electrochem Soc 2010;157(4):A528–35.
[9] Cho Y, Cho J. Significant improvement of $LiNi_{0.8}Co_{0.15}Al_{0.05}O_2$ cathodes at 60 °C by $SiO_2$ dry coating for Li-ion batteries. J Electrochem Soc 2010;157(6):A625–9.
[10] Barnett B, Rempel J, Ofer D, Oh B, Sriramulu S, et al. PhEV battery cost assessment. In: DOE hydrogen program and vehicle technologies program annual merit review and peer evaluation meeting. Washington, DC; June 7–11, 2010.
[11] Strachan PA, Kokogiannakis G, Macdonald IA. History and development of validation with the ESP-r simulation program. Build Environ 2008;43(4):601–9.
[12] Swan LG, Ugursal I, Beausoleil-Morrison I. Hybrid residential end-use energy and greenhouse gas emissions model development and verification for Canada. J Build Perform Sim 2013;6(1):1–23.
[13] Landgrebe AR, Donley SW. Battery storage in residential applications of energy from photovoltaic sources. Appl Energy 1983;15(2):127–37.
[14] Jenkins DP, Fletcher J, Kane D. Model for evaluating impact of battery storage on microgeneration systems in dwellings. Energy Convers Manage 2008;49(8):2413–24.
[15] McKenna E, McManus M, Cooper S, Thomson M. Economic and environmental impact of lead-acid batteries in grid-connected domestic PV systems. Appl Energy 2013;104:239–49.
[16] Ribberink H, Wang W. Improving ESP-rs battery model with active battery life control and coverage of vanadium redox flow batteries. In: Proceedings of the eSim2008 Conf. Quebec City; May 21–11, 2008.
[17] Stadler M, Kloess M, Groissböck M, Cardoso G, Sharma R, Bozchalui MC, et al. Electric storage in California's commercial buildings. Appl Energy 2013;104:711–22.
[18] Saldanha N. Towards the assessment of a residential electric storage system: analysis of Canadian residential electricity use and the development of a lithium-ion battery model [dissertation]. Ottawa (ON): Carleton U; 2010.
[19] Newman J, Tiedemann W. Porous-electrode theory with battery applications. AIChE J 1975;21(1):25–41.
[20] Fuller TF, Doyle M, Newman J. Simulation and optimization of the dual lithium ion insertion cell. J Electrochem Soc 1994;141(1):1–10.
[21] Doyle M, Newman M, Gozdz AS, Schmutz CN, Tarascon JM. Comparison of modeling predictions with experimental data from plastic lithium ion cells. J Electrochem Soc 1996;143(6):1890–903.
[22] Powell IV AC, Arroyave R. Open source software for materials and process modeling. JOM 2008;60(5):32–9.
[23] Gao L, Liu S, Dougal R. Dynamic lithium-ion battery model for system simulation. IEEE Trans Compon Packag Technol 2002;25(3):495–505.
[24] Ramadass P, Haran B, White R, Popov BN. Capacity fade of Sony 18,650 cells cycled at elevated temperatures: Part I. Cycling performance. J Power Sources 2002;112(2):606–13.
[25] Natural Resources Canada. Energy use data handbook 1990 to 2007. Ottawa; 2009. <http://oee.nrcan.gc.ca/publications/statistics/handbook09/pdf/handbook09.pdf.>
[26] Ferguson A, Kelly N, Weber A, Griffith B. Modelling residential-scale combustion-based cogeneration in building simulation. J Build Perform Sim 2009;2(1):1–14.
[27] Environment Canada. Daily data report Ottawa, Ontario. Ottawa, 2010. < http://climate.weatheroffice.gc.ca/>.
[28] Divya KC, Østergaard J. Battery energy storage technology for power systems An overview. Elec Power Sys Res 2009;79(4):511–20.